Supporting Information:

Computational Prediction of the Binding Pose of Metal-Binding Pharmacophores

Johannes Karges, Ryjul W. Stokes, and Seth M. Cohen*

Department of Chemistry and Biochemistry, University of California, San Diego, La Jolla, California 92093, United States

*scohen@ucsd.edu

Table of Contents

EXPERIMENTAL SECTION

Structure Preparation

The geometry of the fragment was determined using density-functional theory (DFT) calculations with the Gaussian software package (Gaussian, Inc., Wallingford CT, 2016). The calculations were performed using the Pople double-zeta basis set with a single set of polarization functions on non-hydrogen atoms (6-31G(d)). Solvent effects were included using a polarizable continuum model (PCM). The structures of all calculated molecules correspond to minima on the ground state potential energy surfaces with no imaginary frequencies present. The metalloprotein structures human carbonic anhydrase II (PDB 6GOT),[1] jumonji-domain of histone lysine demethylase (PDB 5ANQ),[2] and N-terminal domain of the polymerase acidic subunit of the RNA-dependent RNA polymerase of the influenza virus (PDB 6E6W)[3] were downloaded from the Protein Data Bank (https://www.rcsb.org/) and prepared for the docking experiment using the Molecular Operating Environment (MOE, Chemical Computing Group ULC, Montreal, QC, Canada, 2019) software package. Water molecules, other small molecules, inhibitors as well as ions were removed. Hydrogen atoms were added and the side chains protonated at physiological pH.

Protein Sequence Homology

Percent sequence identity and percent sequence coverage was determined using BLAST.[4] hCAII sequences were compared to the sequence of PDB accession code 6RKN. KDM sequences were compared to the sequence of PDB accession code 2VD7. PA_N sequences were compared to the sequence of PDB accession code 6DCZ.

Fragment Docking

The structurally optimized fragments were docked using the Genetic Optimization for Ligand Docking (GOLD, Cambridge Crystallographic Data Centre, Cambridge, United Kingdom, 2019) software package. The protein structure was considered rigid. The binding pose of the compounds was predicted using a genetic algorithm with a population size of 200, selection pressure of 1.2, number of operations of 500000, number of islands of 5, niche size of 2, crossover frequency of 95, mutation frequency of 95, and a migration frequency of 10. The genetic algorithm was set to 100 runs. The metal ions within the active site were predefined to have a tetrahedral geometry for Zn and an octahedral geometry for Fe or Mn. During the docking procedure the binding poses were evaluated using the ChemPLP scoring function. After docking, the obtained solutions were re-scored using the GoldScore fitness function.

Protein Alignment

PDB files and the docking pose from GOLD were loaded into MOE and identical subunits were removed. The sequences were aligned, and the pocket residues were superposed. For $PA_{N,}$ endonuclease, residues 109-119 were superposed with an RMSD of 0.17 Å. The active site alignment was further refined by superposing the proteins using two manganese atoms and the amine in His41 as alignment points, with an RMSD of 0.14 Å (Figure S7a.). For KDM, the sequences were aligned, and the pocket residues were superposed with an RMSD of 0.28 Å. The active site alignment was further refined using the Fe ion, the amine from His188 and the amine in His276 as alignment points, with an RMS distance of 0.13 Å (Figure S7b.). For hCAII, residues the pocket residues were superposed with an RMSD of 0.23 Å, which provided sufficient alignment and did not require further refinement (Figure S7c.).

Fragment Growth

Fragment growth was performed in MOE. The model structure from GOLD was loaded into MOE. The fragment model for each protein was manually extended, and the added group was energy minimized using the Amber10:EHT forcefield with a gradient of 0.1 RMS kcal/mol/Å^2, while the MBP was not altered. For the PA_N model, the atoms in the core of the MBP were manually changed to match the corresponding PDB structure.

Evaluation of binding pose prediction

The binding pose was evaluated by comparing the computationally docked model with the corresponding PDB structure. After the proteins were aligned, poses of the PDB ligand and the computationally-derived ligand were uploaded to the LigRMSD 1.0 server[5] and an RMSD value was calculated.

Docking with AutoDock Vina

The structurally optimized fragments for 2WEJ, 1I9L, 6E6V, and 6E6W were docked using the AutoDock Vina software (version 1.2.0, The Scripps Research Institute, La Jolla CA, 2021). The protein structure was considered rigid. The cubic grid for the docking experiment was chosen so that the whole protein was covered. As default parameters, the energy range was set at 4 and the exhaustiveness at 8. The best scored binding pose was compared with the crystallographically determined binding pose.

Docking with SwissDock

The structurally optimized fragments 2WEJ, 1I9L, 6E6V, and 6E6W were docked using SwissDock (Swiss Institute of Bioinformatics, Lausanne, 2021). The protein structure was

considered rigid. No information about the binding pocket was provided, allowing docking towards the whole protein. The best scored binding pose was compared with the crystallographically determined binding pose.

SUPPORTING FIGURES AND TABLES

Table S1. Percent sequence identity and percent sequence coverage between proteins.

Protein	PDB	Percent Identity	Percent Coverage	Protein	PDB	Percent Identity	Percent Coverage	Protein	PDB	Percent Identity	Percent Coverage
hCAII	**4MTY**	**Parent**	**Parent**	**KDM**	**2VD7**	**Parent**	**Parent**	**PA_N**	**6DCZ**	**Parent**	**Parent**
	1IF8	100	99		3PDQ	100	100		4E5I	92.97	96
	1I9L	99	99		4GD4	100	100		4E5J	92.97	96
	2HD6	100	99		4URA	100	94		6E3M	100	100
	1KWR	100	100		5A7N	100	100		6E3N	100	100
	3K34	100	100		5A7O	99.74	100		6E3O	100	100
	3MNA	100	100		5A7P	100	100		6E3P	100	100
	3MMF	100	100		5A7Q	100	100		6E4C	100	100
	3MZC	100	100		5A7S	100	100		6E6V	100	100
	3NON	100	100		5A7W	99.74 - 100*	100		6E6W	100	100
	3N4B	100	100		5A80	100	100				
	4ILX	100	98		5ANQ	100	94				
	4ITP	100	98		5F5I	100	95				
	4XE1	100	100		5VMP	97.33	98				
	5BYI	100	100		6CG2	100	91				
	5E2R	100	100								
	5LJK	100	99								
	5N1S	100	100								
	5N1R	100	100								
	5N24	100	100								
	6EQU	100	100								
	6IOW	100	100								
	6SDS	100	100								

***** Two different sequences reported in PDB accession code 5A7W.

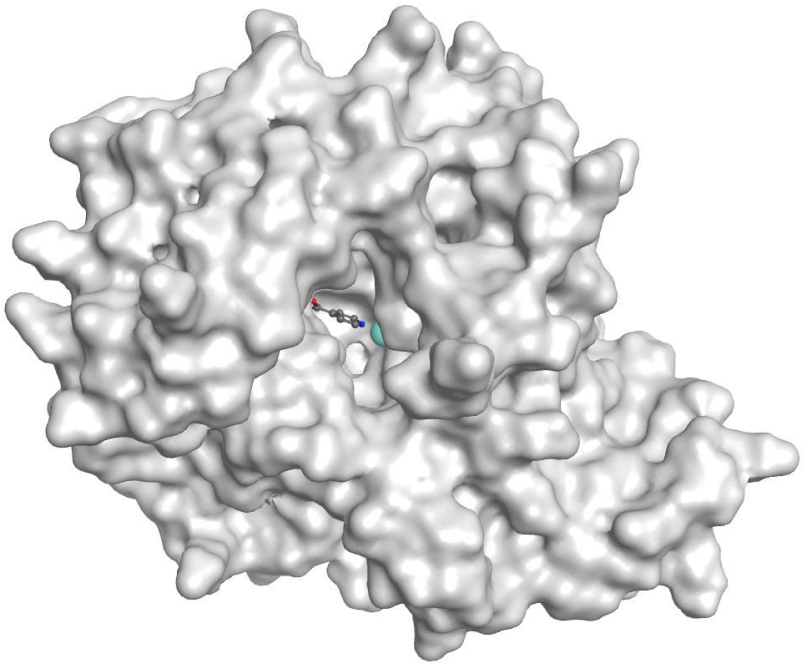

a)

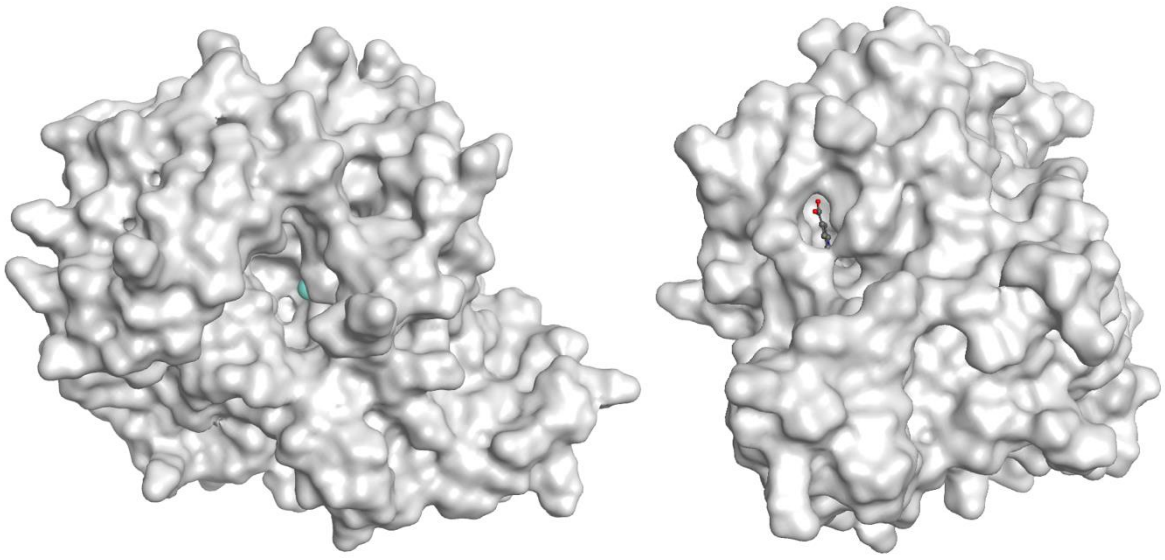

b)

Figure S1. Binding pose of MBP 2,4-pyridinedicarboxylic acid: a) restricted to a box of 20 Å centered around the KDM active site metal ion (where the MBP ultimately binds), or b) without any restrictions. Without any restrictions, the MBP does not bind at the active site (left), but rather at a distal site (right, protein image rotated ~120° to show docked site) in KDM. The distal site is Protein (PA_N) shown as gray surface, active site metals shown as cyan surface, and MBP shown as sticks colored by atom type.

MBP Fragment

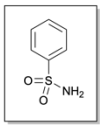

Full Length Inhibitors

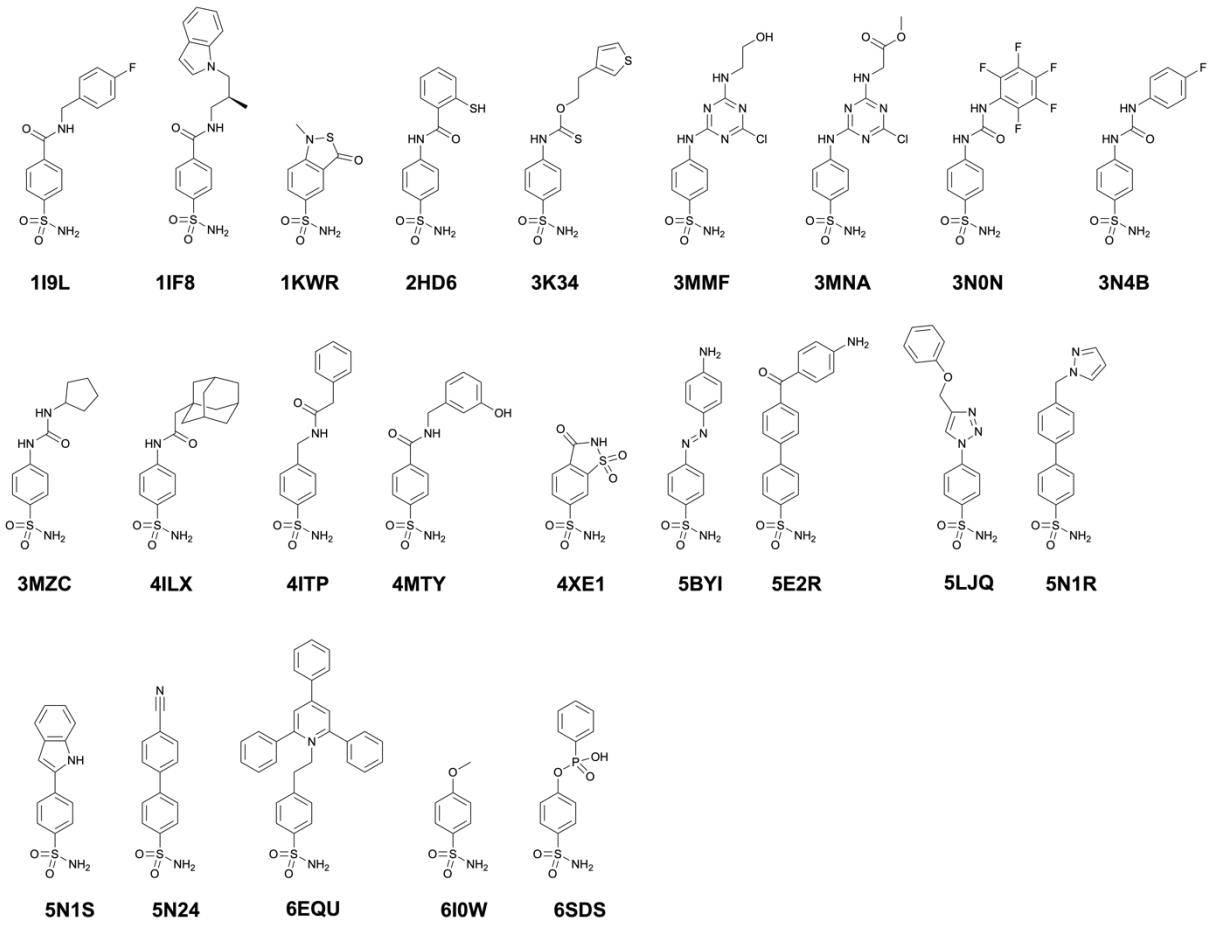

Figure S2. Chemical Structures of the docked fragment as well as full length inhibitors for hCAII. Inhibitor naming is associated with their corresponding PDB accession code.[6-23]

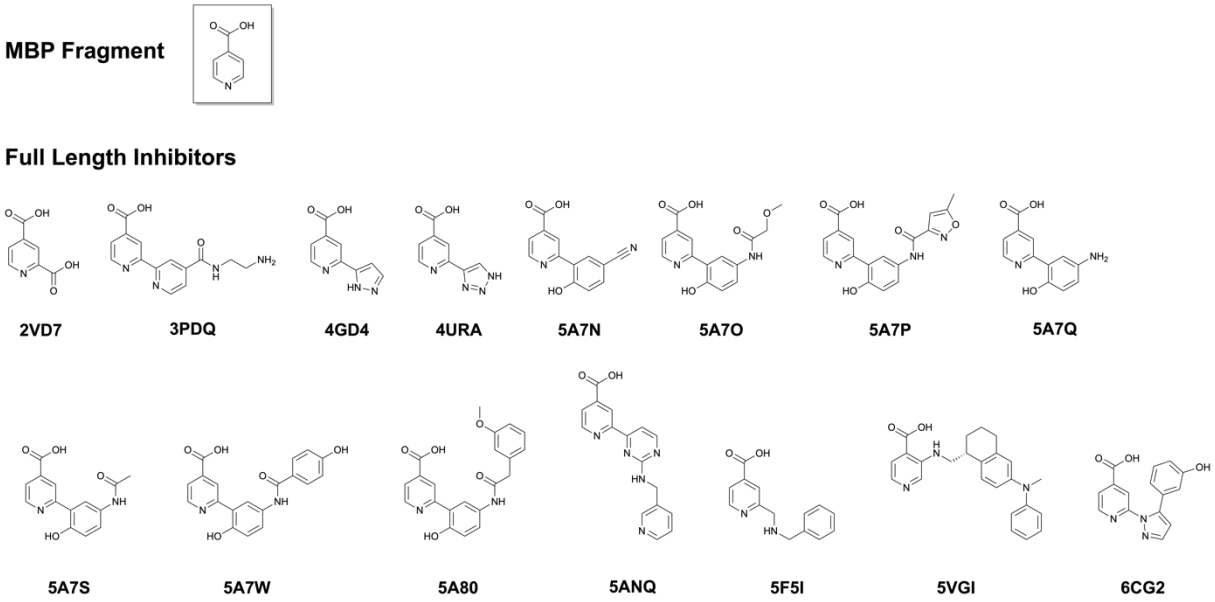

Figure S3. Chemical Structures of the docked fragment as well as full length inhibitors for KDM. Inhibitor naming is associated with their corresponding PDB accession code.[2, 24-31]

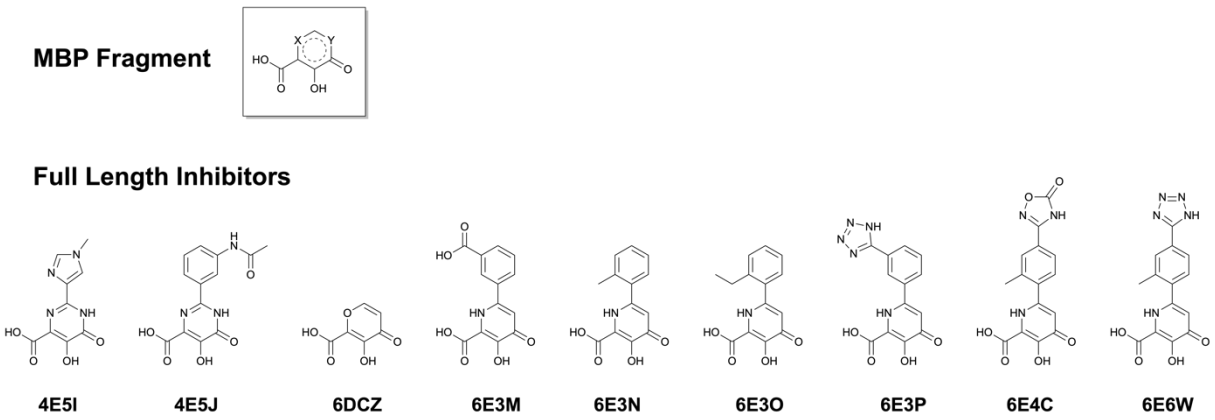

Figure S4. Chemical Structures of the docked fragment as well as full length inhibitors for PA_N. Inhibitor naming is associated with their corresponding PDB accession code.[3, 32-33]

Table S2. Root-mean-square deviation of atomic positions (RMSD) between the computational model and the MBP of the evaluated PDB structures.

Protein	**PDB ID**	**RMSD**	**Protein**	**PDB ID**	**RMSD**	**Protein**	**PDB ID**	**RMSD**
hCAII	**Model**		**KDM**	**Model**		**PA_N**	**Model**	
	1I9L	0.71		2VD7	0.5		4E5J	1.14
	1IF8	0.85		3PDQ	0.22		4E5I	1.92
	1KWR	0.87		4GD4	0.69		6E4C	0.36
	2HD6	0.91		4URA	0.69		6E3N	0.42
	3K34	0.86		5A7N	0.23		6DCZ	0.69
	3MMF	0.76		5A7O	0.47		6E3M	1.07
	3MNA	0.77		5A7P	0.44		6E6W	0.30
	3MZC	1.01		5A7Q	0.93		6E3P	0.76
	3N0N	0.91		5A7S	0.76		6E3O	0.33
	3N4B	0.93		5A7W	0.45		Average	0.78
	4ILX	0.97		5A80	0.47			
	4ITP	0.79		5ANQ	0.24			
	4MTY	0.84		5F5I	0.56			
	4XE1	1.08		5VGI	0.71			
	5BYI	0.86		6CG2	0.46			
	5E2R	1.02		Average	0.52			
	5N1R	1.03						
	5N24	1.10						
	6EQU	0.96						
	6I0W	0.77						
	6SDS	0.79						
	Average	0.90						

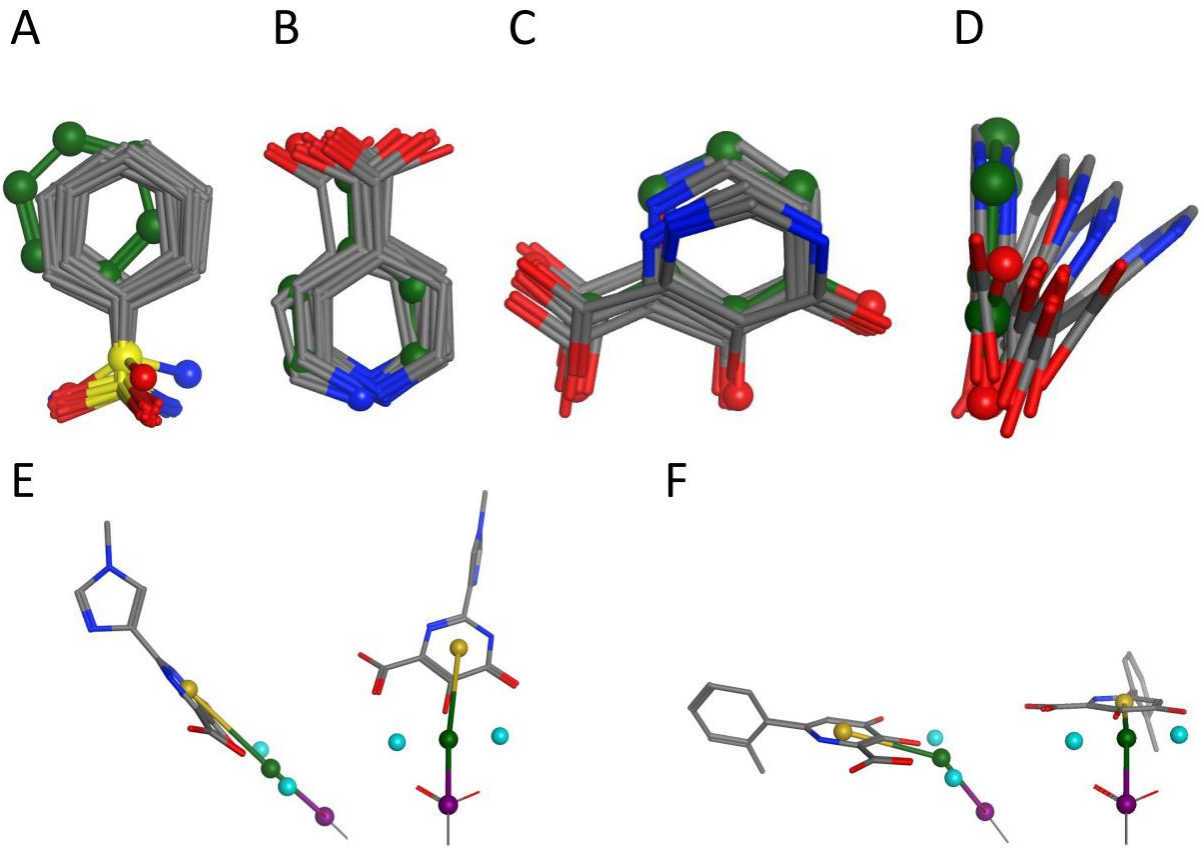

Figure S5. Overlay between the docked MBP using GOLD (green) and the MBP fragment from the corresponding PDB structures for: (A) hCAII, (B) KDM, (C) PA_N, and (D) PA_N (perspective of this pose is rotated by 90° compared to the other images to highlight the 'tilt' of the MBP poses). Angle between the carbon atom of the carboxyl group of Asp108 (purple), a centroid between both metal centers (green), and a centroid of the aromatic MBP moiety (yellow) for (E) 4E5I (175° binding angle) and (F) 6E3N (145° binding angle).

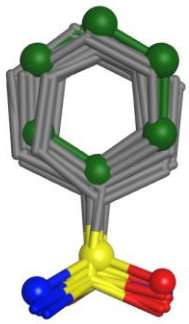

Figure S6. Overlay between the computationally docked MBP (green) and corresponding MBPs from PDB structures for hCAII (gray). Using a modified scoring function with a metal-binding bias the benzenesulfonamide MBP is much better aligned with the experimentally determined structures (compare with Figure S5A).

Table S3. Root-mean-square deviation of atomic positions (RMSD) between the computational model using a scoring function with a metal-binding bias and only the MBP of the evaluated PDB structures.

Protein	**PDB ID**	**RMSD**
hCAII	**Model**	
	1I9L	0.41
	1IF8	0.60
	1KWR	0.34
	2HD6	0.46
	3K34	0.42
	3MMF	0.30
	3MNA	0.27
	3MZC	0.42
	3N0N	0.34
	3N4B	0.38
	4ILX	0.34
	4ITP	0.29
	4MTY	0.46
	4XE1	0.51
	5BYI	0.51
	5E2R	0.53
	5LJQ	0.38
	5N1R	1.19
	5N1S	0.52
	5N24	0.53
	6EQU	0.48
	6I0W	0.56
	6SDS	0.53
	Average	0.47

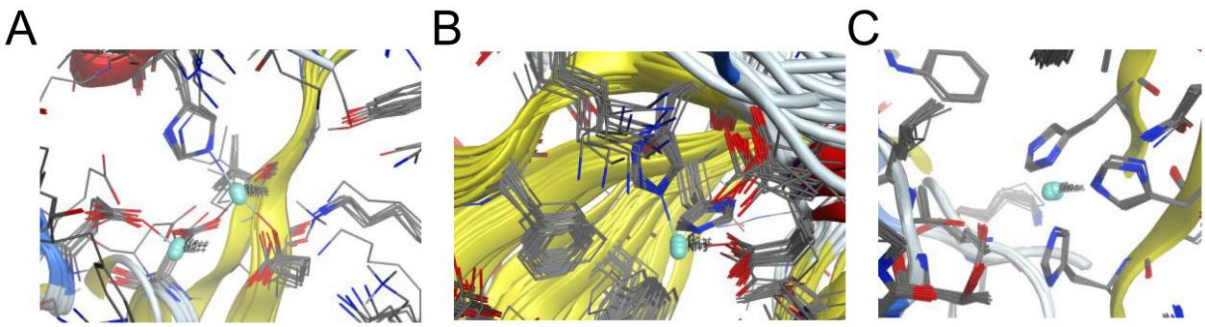

Figure S7. Active site alignment for: (A) PA_N, (B) KDM, and (C) hCAII.

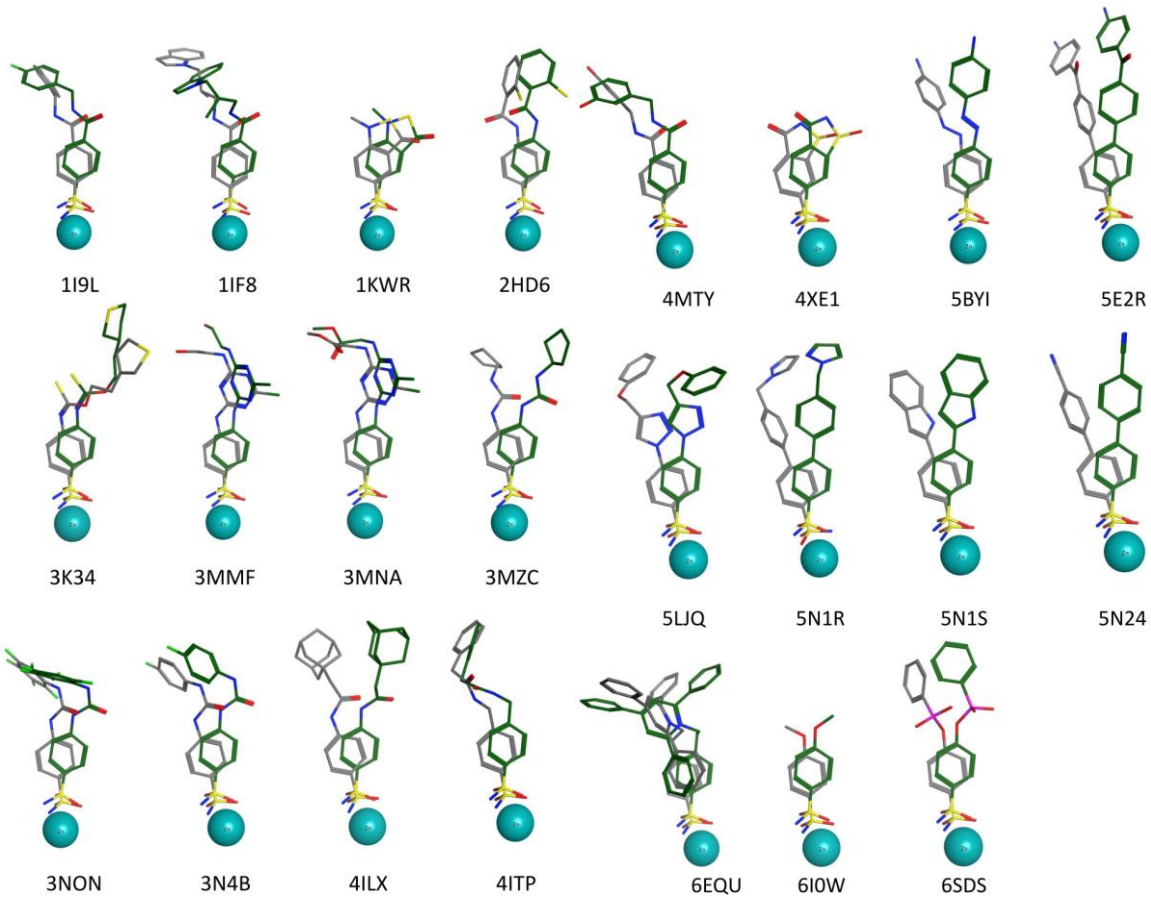

Figure S8. Comparison of binding modes of computationally derived hCAII inhibitor poses (green) and crystallographically determined structures (gray) from PDB entries (PDB entry codes shown).

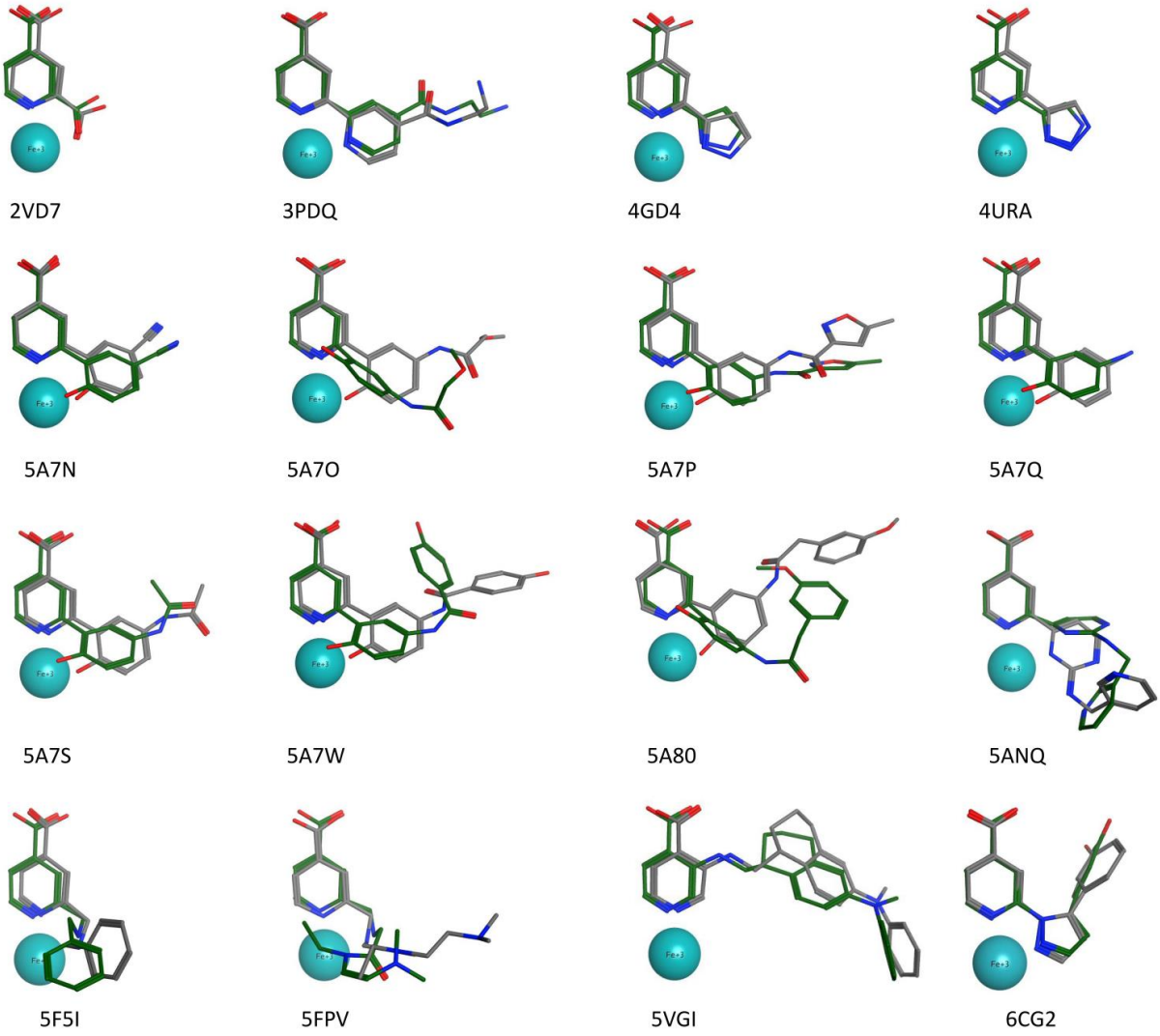

Figure S9. Comparison of binding modes of computationally derived KDM inhibitor poses (green) and crystallographically determined structures (gray) from PDB entries (PDB entry codes shown).

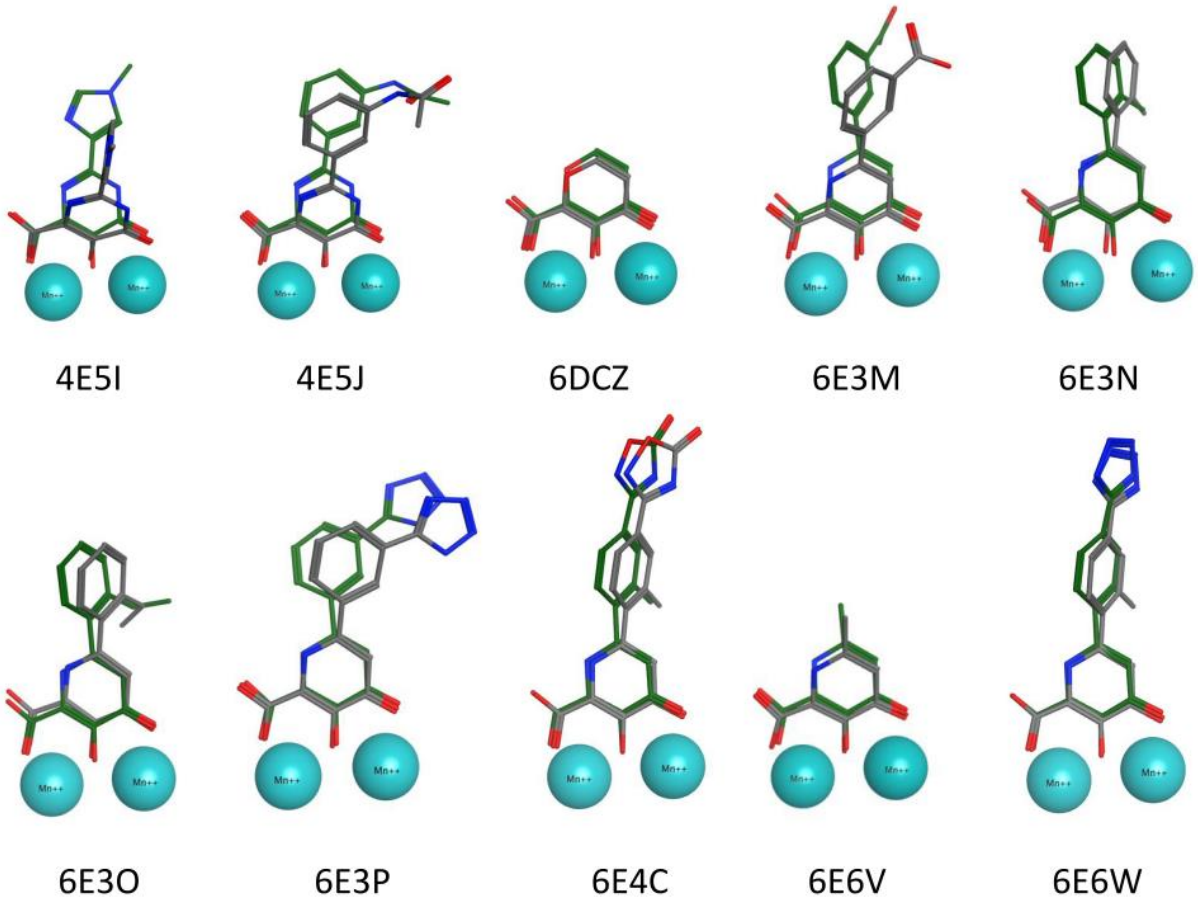

Figure S10. Comparison of binding modes of computationally derived PA_N inhibitor poses (green) and crystallographically determined structures (gray) from PDB entries (PDB entry codes shown).

Table S4. RMSD values of computationally and crystallographically determined full-length inhibitors of the enzyme-inhibitor complexes.

Enzyme	Entry	RMSD	Reference
hCAII	1I9L	1.69	6
	1IF8	3.18	7
	1KWR	1.07	8
	2HD6	1.74	9
	3K34	1.91	10
	3MMF	1.67	11
	3MNA	1.20	11
	3N0N	3.79	12
	3N4B	3.03	12
	3MZC	3.73	12
	4ILX	4.11	13
	4ITP	0.95	14
	4MTY	1.86	15
	4XE1	1.33	16
	5BYI	2.79	17
	5E2R	3.07	18
	5LJQ	4.58	19
	5N1R	2.80	20
	5N1S	2.87	20
	5N24	2.61	20
	6EQU	2.48	21
	6I0W	1.24	22
	6SDS	2.35	23
	Average	2.44	
KDM	2VD7	0.52	24
	3PDQ	0.85	25
	4GD4	0.69	26
	4URA	0.67	27
	5A7N	1.04	28
	5A7O	2.77	28
	5A7P	1.30	28
	5A7Q	1.02	28
	5A7S	1.32	28
	5A7W	2.70	28
	5A80	3.92	28
	5ANQ	2.10	2
	5F5I	1.42	29
	5VGI	1.79	31
	6CG2	1.46	30-31
	Average	1.57	
PA_N	4E5I	4.22	32
	4E5J	3.05	32
	6DCZ	0.69	33
	6E3M	2.61	3
	6E3N	0.65	3
	6E3O	0.83	3
	6E3P	2.09	3
	6E4C	0.57	3
	6E6W	0.39	3
	Average	1.60	

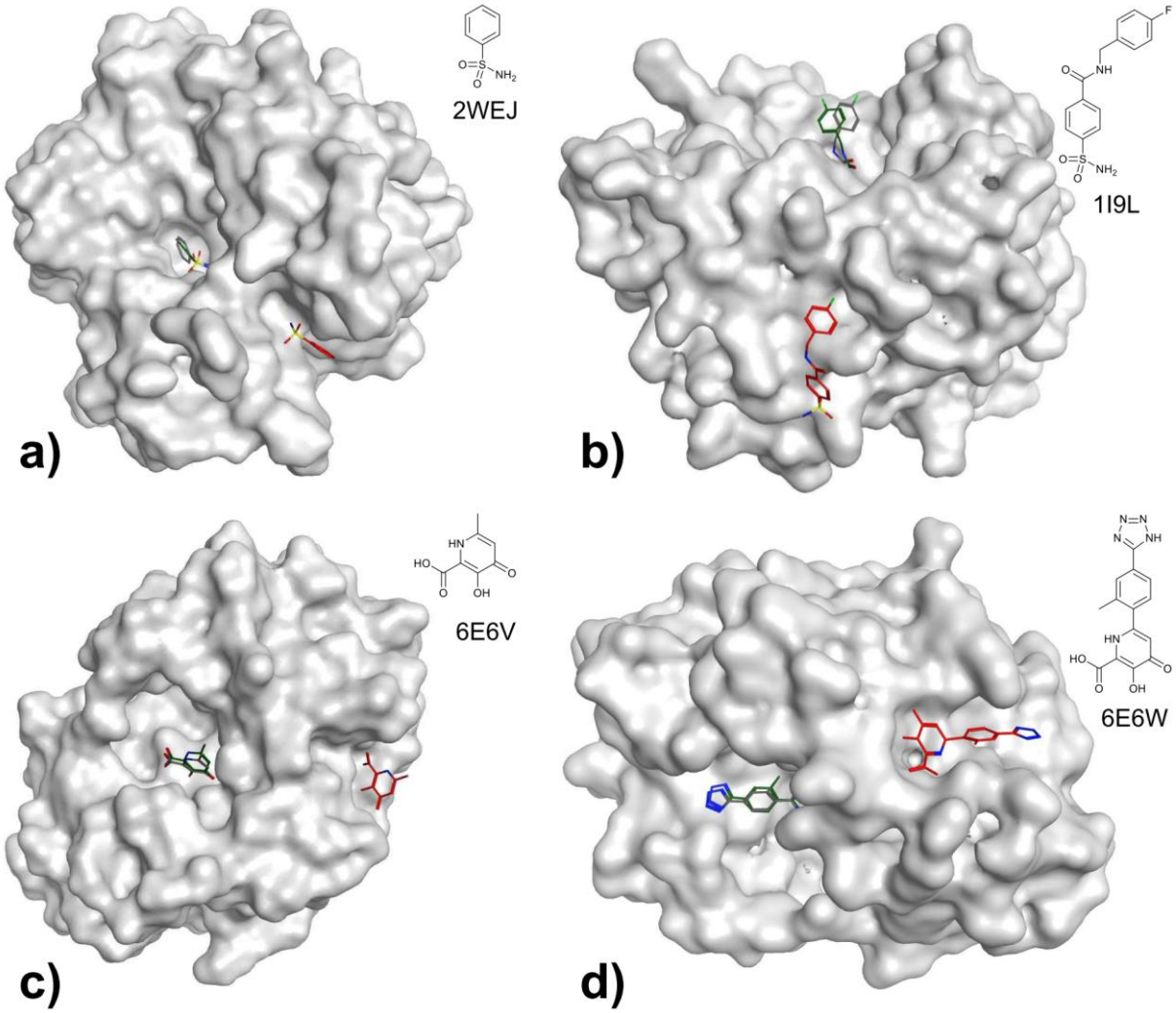

Figure S11. Comparison of binding modes of computationally derived hCAII inhibitor poses upon docking with AutoDock Vina (red), our reported docking procedure (green), and crystallographically determined structures (gray) from PDB entries: a) 2WEJ, b) 1I9L, c) 6E6V, d) 6E6W.

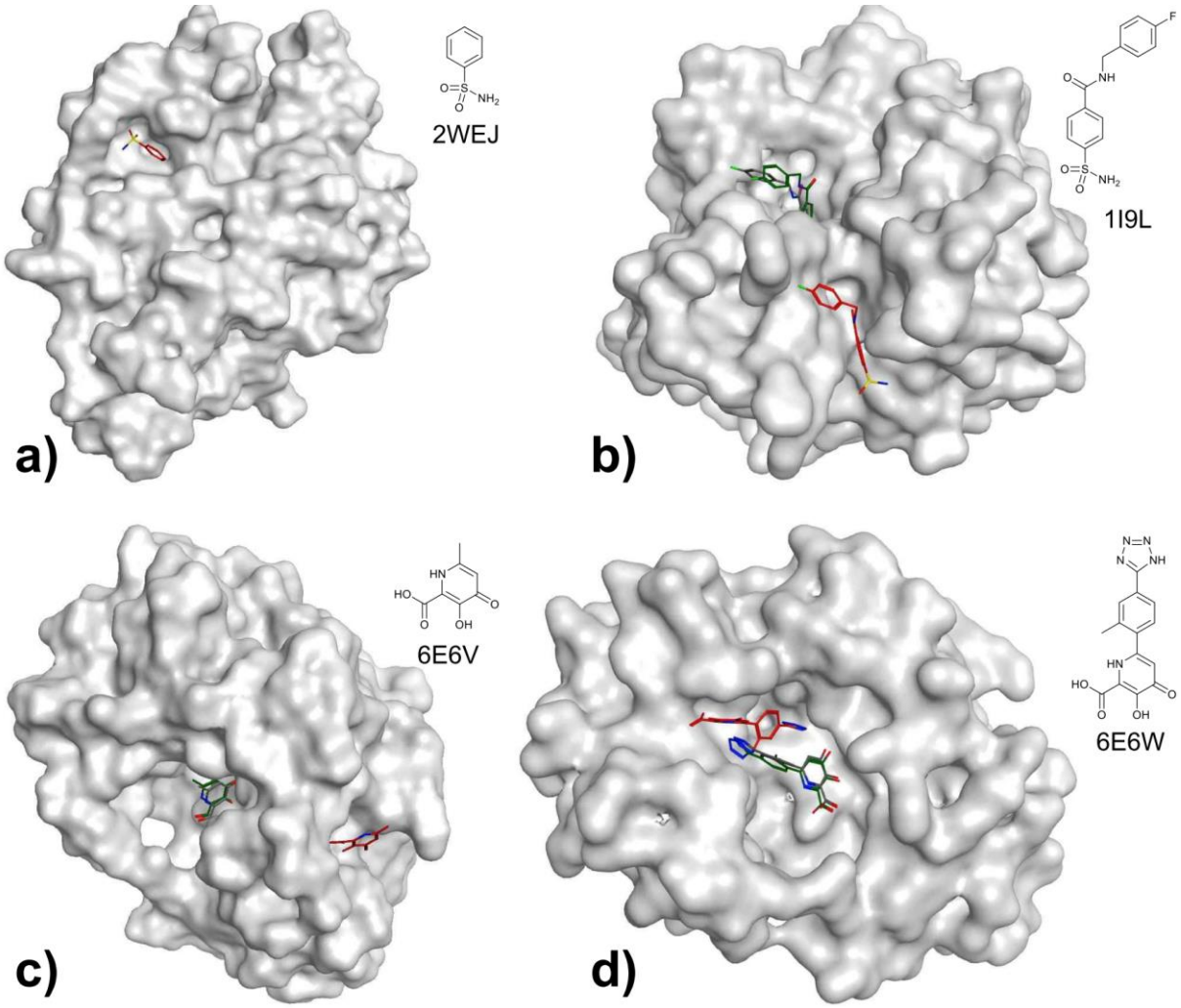

Figure S12. Comparison of binding modes of computationally derived PA_N inhibitor poses upon docking with SwissDock (red), our reported docking procedure (green), and crystallographically determined structures (gray) from PDB entries: a) 2WEJ (the active site is found on the other side of this protein and therefore only the with SwissDock determined binding pose can be seen), b) 1I9L, c) 6E6V, d) 6E6W.

REFERENCES

1. Angeli, A.; Tanini, D.; Capperucci, A.; Malevolti, G.; Turco, F.; Ferraroni, M.; Supuran, C. T., Synthesis Of Different Thio-Scaffolds Bearing Sulfonamide With Subnanomolar Carbonic Anhydrase II And IX Inhibitory Properties And X-ray Investigations For Their Inhibitory Mechanism. *Bioorg. Chem.* **2018,** *81*, 642-648.

2. Roatsch, M.; Robaa, D.; Pippel, M.; Nettleship, J. E.; Reddivari, Y.; Bird, L. E.; Hoffmann, I.; Franz, H.; Owens, R. J.; Schüle, R.; Flaig, R.; Sippl, W.; Jung, M., Substituted 2-(2-aminopyrimidin-4-yl)pyridine-4-carboxylates As Potent Inhibitors Of JumonjiC Domain-Containing Histone Demethylases. *Future Med. Chem.* **2016,** *8* (13), 1553-1571.

3. Credille, C. V.; Morrison, C. N.; Stokes, R. W.; Dick, B. L.; Feng, Y.; Sun, J.; Chen, Y.; Cohen, S. M., SAR Exploration Of Tight-Binding Inhibitors Of Influenza Virus PA Endonuclease. *J. Med. Chem.* **2019,** *62* (21), 9438-9449.

4. Altschul, S. F.; Gish, W.; Miller, W.; Myers, E. W.; Lipman, D. J., Basic Local Alignment Search Tool. *J. Mol. Biol.* **1990,** *215* (3), 403-410.

5. Velázquez-Libera, J. L.; Durán-Verdugo, F.; Valdés-Jiménez, A.; Núñez-Vivanco, G.; Caballero, J., LigRMSD: A Web Server For Automatic Structure Matching And RMSD Calculations Among Identical And Similar Compounds In Protein-Ligand Docking. *Bioinformatics* **2020,** *36* (9), 2912-2914.

6. Kim, C.-Y.; Chandra, P. P.; Jain, A.; Christianson, D. W., Fluoroaromatic−Fluoroaromatic Interactions Between Inhibitors Bound In The Crystal Lattice Of Human Carbonic Anhydrase II. *J. Am. Chem. Soc.* **2001,** *123* (39), 9620-9627.

7. Grzybowski, B. A.; Ishchenko, A. V.; Kim, C.-Y.; Topalov, G.; Chapman, R.; Christianson, D. W.; Whitesides, G. M.; Shakhnovich, E. I., Combinatorial Computational Method Gives New Picomolar Ligands For A Known Enzyme. *Proc. Natl. Acad. Sci.* **2002,** *99* (3), 1270-1273.

8. Grüneberg, S.; Stubbs, M. T.; Klebe, G., Successful Virtual Screening For Novel Inhibitors Of Human Carbonic Anhydrase: Strategy And Experimental Confirmation. *J. Med. Chem.* **2002,** *45* (17), 3588-3602.

9. De Simone, G.; Vitale, R. M.; Di Fiore, A.; Pedone, C.; Scozzafava, A.; Montero, J.-L.; Winum, J.-Y.; Supuran, C. T., Carbonic Anhydrase Inhibitors: Hypoxia-Activatable Sulfonamides Incorporating Disulfide Bonds That Target the Tumor-Associated Isoform IX. *J. Med. Chem.* **2006,** *49* (18), 5544-5551.

10. Behnke, C. A.; Le Trong, I.; Godden, J. W.; Merritt, E. A.; Teller, D. C.; Bajorath, J.; Stenkamp, R. E., Atomic Resolution Studies Of Carbonic Anhydrase II. *Acta Crystallogr. D* **2010,** *66* (5), 616-627.

11. Carta, F.; Garaj, V.; Maresca, A.; Wagner, J.; Avvaru, B. S.; Robbins, A. H.; Scozzafava, A.; McKenna, R.; Supuran, C. T., Sulfonamides Incorporating 1,3,5-Triazine Moieties Selectively And Potently Inhibit Carbonic Anhydrase Transmembrane Isoforms IX, XII And XIV Over Cytosolic Isoforms I And II: Solution And X-ray Crystallographic Studies. *Bioorg. Med. Chem.* **2011,** *19* (10), 3105-3119.

12. Pacchiano, F.; Aggarwal, M.; Avvaru, B. S.; Robbins, A. H.; Scozzafava, A.; McKenna, R.; Supuran, C. T., Selective Hydrophobic Pocket Binding Observed Within The Carbonic Anhydrase II Active Site Accommodate Different 4-Substituted-Ureido-Benzenesulfonamides And Correlate To Inhibitor Potency. *Chem. Commun.* **2010,** *46* (44), 8371-8373.

13. Biswas, S.; Carta, F.; Scozzafava, A.; McKenna, R.; Supuran, C. T., Structural Effect Of Phenyl Ring Compared To Thiadiazole Based Adamantyl-Sulfonamides On Carbonic Anhydrase Inhibition. *Bioorg. Med. Chem.* **2013,** *21* (8), 2314-2318.

14. Güzel-Akdemir, Ö.; Biswas, S.; Lastra, K.; McKenna, R.; Supuran, C. T., Structural Study Of The Location Of The Phenyl Tail Of Benzene Sulfonamides And The Effect On Human Carbonic Anhydrase Inhibition. *Bioorg. Med. Chem.* **2013,** *21* (21), 6674-6680.

15. Buratto, J.; Colombo, C.; Stupfel, M.; Dawson, S. J.; Dolain, C.; Langlois d'Estaintot, B.; Fischer, L.; Granier, T.; Laguerre, M.; Gallois, B.; Huc, I., Structure Of A Complex Formed By A Protein And A Helical Aromatic Oligoamide Foldamer At 2.1 Å Resolution. *Angew. Chem. Int. Ed.* **2014,** *53* (3), 883-887.

16. Alterio, V.; Tanc, M.; Ivanova, J.; Zalubovskis, R.; Vozny, I.; Monti, S. M.; Di Fiore, A.; De Simone, G.; Supuran, C. T., X-ray Crystallographic And Kinetic Investigations Of 6-Sulfamoyl-Saccharin As A Carbonic Anhydrase Inhibitor. *Org. Biomol. Chem.* **2015,** *13* (13), 4064-4069.

17. Runtsch, L. S.; Barber, D. M.; Mayer, P.; Groll, M.; Trauner, D.; Broichhagen, J., Azobenzene-Based Inhibitors Of Human Carbonic Anhydrase II. *Beilstein J. Org. Chem.* **2015,** *11*, 1129-1135.

18. La Regina, G.; Coluccia, A.; Famiglini, V.; Pelliccia, S.; Monti, L.; Vullo, D.; Nuti, E.; Alterio, V.; De Simone, G.; Monti, S. M.; Pan, P.; Parkkila, S.; Supuran, C. T.; Rossello, A.; Silvestri, R., Discovery Of 1,1′ -Biphenyl-4-Sulfonamides As A New Class Of Potent And Selective Carbonic Anhydrase XIV Inhibitors. *J. Med. Chem.* **2015,** *58* (21), 8564-8572.

19. Nocentini, A.; Ferraroni, M.; Carta, F.; Ceruso, M.; Gratteri, P.; Lanzi, C.; Masini, E.; Supuran, C. T., Benzenesulfonamides Incorporating Flexible Triazole Moieties Are Highly Effective Carbonic Anhydrase Inhibitors: Synthesis And Kinetic, Crystallographic, Computational, And Intraocular Pressure Lowering Investigations. *J. Med. Chem.* **2016,** *59* (23), 10692-10704.

20. Ferraroni, M.; Cornelio, B.; Sapi, J.; Supuran, C. T.; Scozzafava, A., Sulfonamide Carbonic Anhydrase Inhibitors: Zinc Coordination And Tail Effects Influence Inhibitory Efficacy And Selectivity For Different Isoforms. *Inorg. Chim. Acta* **2018,** *470*, 128-132.

21. Alterio, V.; Esposito, D.; Monti, S. M.; Supuran, C. T.; De Simone, G., Crystal Structure Of The Human Carbonic Anhydrase II Adduct With 1-(4-sulfamoylphenyl-ethyl)-

2,4,6-triphenylpyridinium Perchlorate, A Membrane-Impermeant, Isoform Selective Inhibitor. *J. Enzyme Inhib. Med. Chem.* **2018,** *33* (1), 151-157.

22. Glöckner, S.; Ngo, K.; Sager, C. P.; Hüfner-Wulsdorf, T.; Heine, A.; Klebe, G., Conformational Changes In Alkyl Chains Determine The Thermodynamic And Kinetic Binding Profiles Of Carbonic Anhydrase Inhibitors. *ACS Chem. Biol.* **2020,** *15* (3), 675-685.

23. Nocentini, A.; Alterio, V.; Bua, S.; Micheli, L.; Esposito, D.; Buonanno, M.; Bartolucci, G.; Osman, S. M.; Alothman, Z. A.; Cirilli, R.; Pierini, M.; Monti, S. M.; Di Cesare Mannelli, L.; Gratteri, P.; Ghelardini, C.; De Simone, G.; Supuran, C. T., Phenyl(thio)phosphon(amid)ate Benzenesulfonamides As Potent And Selective Inhibitors Of Human Carbonic Anhydrases II And VII Counteract Allodynia In A Mouse Model Of Oxaliplatin-Induced Neuropathy. *J. Med. Chem.* **2020,** *63* (10), 5185-5200.

24. Rose, N. R.; Ng, S. S.; Mecinović, J.; Liénard, B. M. R.; Bello, S. H.; Sun, Z.; McDonough, M. A.; Oppermann, U.; Schofield, C. J., Inhibitor Scaffolds For 2-Oxoglutarate-Dependent Histone Lysine Demethylases. *J. Med. Chem.* **2008,** *51* (22), 7053-7056.

25. Chang, K.-H.; King, O. N. F.; Tumber, A.; Woon, E. C. Y.; Heightman, T. D.; McDonough, M. A.; Schofield, C. J.; Rose, N. R., Inhibition Of Histone Demethylases By 4-Carboxy-2,2′ -Bipyridyl Compounds. *ChemMedChem* **2011,** *6* (5), 759-764.

26. King, O. N. F.; Krojer, T.; Arrowsmith, C. H.; Edwards, A.; Bountra, C.; McDonough, M. A.; Schofield, C. J., Crystal Structure Of JMJD2A Complexed With Inhibitor. to be published, PDB Code: 4GD4.

27. England, K. S.; Tumber, A.; Krojer, T.; Scozzafava, G.; Ng, S. S.; Daniel, M.; Szykowska, A.; Che, K.; von Delft, F.; Burgess-Brown, N. A.; Kawamura, A.; Schofield, C. J.; Brennan, P. E., Optimisation Of A Triazolopyridine Based Histone Demethylase Inhibitor Yields A Potent And Selective KDM2A (FBXL11) Inhibitor. *Med. Chem. Commun.* **2014,** *5* (12), 1879-1886.

28. Korczynska, M.; Le, D. D.; Younger, N.; Gregori-Puigjané, E.; Tumber, A.; Krojer, T.; Velupillai, S.; Gileadi, C.; Nowak, R. P.; Iwasa, E.; Pollock, S. B.; Ortiz Torres, I.; Oppermann, U.; Shoichet, B. K.; Fujimori, D. G., Docking And Linking Of Fragments To Discover Jumonji Histone Demethylase Inhibitors. *J. Med. Chem.* **2016,** *59* (4), 1580-1598.

29. Bavetsias, V.; Lanigan, R. M.; Ruda, G. F.; Atrash, B.; McLaughlin, M. G.; Tumber, A.; Mok, N. Y.; Le Bihan, Y.-V.; Dempster, S.; Boxall, K. J.; Jeganathan, F.; Hatch, S. B.; Savitsky, P.; Velupillai, S.; Krojer, T.; England, K. S.; Sejberg, J.; Thai, C.; Donovan, A.; Pal, A.; Scozzafava, G.; Bennett, J. M.; Kawamura, A.; Johansson, C.; Szykowska, A.; Gileadi, C.; Burgess-Brown, N. A.; von Delft, F.; Oppermann, U.; Walters, Z.; Shipley, J.; Raynaud, F. I.; Westaway, S. M.; Prinjha, R. K.; Fedorov, O.; Burke, R.; Schofield, C. J.; Westwood, I. M.; Bountra, C.; Müller, S.; van Montfort, R. L. M.; Brennan, P. E.; Blagg, J., 8-Substituted Pyrido[3,4-d]pyrimidin-4(3H)-one Derivatives As Potent, Cell Permeable, KDM4 (JMJD2) And KDM5 (JARID1) Histone Lysine Demethylase Inhibitors. *J. Med. Chem.* **2016,** *59* (4), 1388-1409.

30. Nie, Z.; Shi, L.; Lai, C.; O'Connell, S. M.; Xu, J.; Stansfield, R. K.; Hosfield, D. J.; Veal, J. M.; Stafford, J. A., Structure-Based Design And Discovery Of Potent And Selective KDM5 Inhibitors. *Bioorg. Med. Chem. Lett.* **2018,** *28* (9), 1490-1494.

31. Chen, Y. K.; Bonaldi, T.; Cuomo, A.; Del Rosario, J. R.; Hosfield, D. J.; Kanouni, T.; Kao, S.-c.; Lai, C.; Lobo, N. A.; Matuszkiewicz, J.; McGeehan, A.; O'Connell, S. M.; Shi, L.; Stafford, J. A.; Stansfield, R. K.; Veal, J. M.; Weiss, M. S.; Yuen, N. Y.; Wallace, M. B., Design Of KDM4 Inhibitors With Antiproliferative Effects In Cancer Models. *ACS Med. Chem. Lett.* **2017,** *8* (8), 869-874.

32. DuBois, R. M.; Slavish, P. J.; Baughman, B. M.; Yun, M.-K.; Bao, J.; Webby, R. J.; Webb, T. R.; White, S. W., Structural And Biochemical Basis For Development Of Influenza Virus Inhibitors Targeting The PA Endonuclease. *PLoS Pathog.* **2012,** *8* (8), e1002830.

33. Credille, C. V.; Dick, B. L.; Morrison, C. N.; Stokes, R. W.; Adamek, R. N.; Wu, N. C.; Wilson, I. A.; Cohen, S. M., Structure–Activity Relationships In Metal-Binding Pharmacophores For Influenza Endonuclease. *J. Med. Chem.* **2018,** *61* (22), 10206-10217.